Available online at www.sciencedirect.com
ScienceDirect
Journal of Solid State Chemistry 179 (2006) 3065–3072
JOURNAL OF SOLID STATE CHEMISTRY
www.elsevier.com/locate/jssc

# Structural investigations of lead–strontium fluoroapatites

Béchir Badraoui[a], Abdallah Aissa[a], Adriana Bigi[b], Mongi Debbabi[a], Massimo Gazzano[b,*]

[a]*Laboratoire de Physico-Chimie des Matériaux, Ecole Nationale d'Ingénieurs de Monastir, 5019 Monastir, Tunisie*
[b]*Dipartimento di Chimica "G. Ciamician", Università degli Studi, and Istituto per la Sintesi Organica e la Fotoreattività, CNR, Via Selmi2, 40126 Bologna, Italy*

Received 27 March 2006; received in revised form 30 May 2006; accepted 1 June 2006
Available online 12 June 2006

**Abstract**

Solid solutions in the system $Pb_{(10-x)}Sr_x(PO_4)_6F_2$, $0 \leqslant x \leqslant 10$, were obtained as apatitic phases from aqueous medium. They were investigated by X-ray diffraction, chemical analysis and infrared (IR) spectroscopy. The results of the structural refinements indicated that the substitution of lead by strontium induces a regular decrease of the lattice constant "*a*" and a preferential strontium distribution in site *M*(1). A progressive shift of the $F^-$ ion position along the apatitic channel was detected and confirmed by IR evidence. The different character of the *M*–F and *M*–O interactions was invoked to justify the structural differences observed as a function of composition.


*Keywords:* Fluoroapatite; Rietveld refinement; Isomorphous substitution

## 1. Introduction

Due to the high flexibility of their structures, and to the wide range of potential practical applications, apatites have long been the subject of scientific investigation. Starting from the work of mineralogists on the different compounds of this kind found in nature, there have been many approaches of solid state chemists to synthesize isotypic compounds with formula $M_5(XO_4)_3Y$. *M* can be replaced by a number of bivalent cations $Ca^{2+}$, $Sr^{2+}$, $Ba^{2+}$, $Cd^{2+}$, $Pb^{2+}$, but monovalent and trivalent cations such as $Na^+$, $K^+$ and $Al^{3+}$ can be hosted as well; $XO_4$ is usually $PO_4^{3-}$, $VO_4^{3-}$ or $AsO_4^{3-}$, but the possible substitutions include also $SiO_4^{4-}$, $CO_3^{2-}$ and $SO_4^{2-}$; *Y* is a monovalent anion, $OH^-$, $F^-$, $Cl^-$, $Br^-$ [1–4]. The great variety of cationic and anionic substitutions is justified by the "open structure" of apatite. In the apatite structure, the Ca ions occupy two types of nonequivalent sites: in *M*(1), Ca ions are aligned in columns and surrounded by nine oxygen atoms at the four-fold symmetry 4*f* position, while in *M*(2) Ca ions are arranged in equilateral triangles centred on the screw axes, and are surrounded by seven oxygen atoms at the six-fold symmetry 6*h* position [1,4]. The physico-chemical properties of the isomorphous derivatives are greatly influenced by the kind and extent of substitution. In view of their possible applications, the interest towards ionic substitutions spans through several fields, from catalysis to medicine, to biology and the environment [5–7]. In particular, ionic substitutions are involved in dental and bone pathologies, in the preparation of bioceramics for hard tissues repair, in possible pollution of phosphate fertilizers, in ionic exchange of apatite-based materials for water treatment and radioactive waste confinements, as well as in the catalytic and luminescent properties of apatites [8–14].

Among the possible monovalent anions, which occupy the channel site formed along the *c*-axis by the Ca(2) ions, the one that best fits into it is fluoride. The ionic radius of fluoride is small enough to permit it to occupy the most symmetric position in the channel (i.e., on mirror planes perpendicular to the *c*-axis), and thus fluorapatite is the apatite with the highest symmetry [15]. Fluorapatite $Ca_{10}(PO_4)_6F_2$ (FAp) is less soluble than hydroxyapatite in acidic solution, and it has been investigated as alternative material for biomedical applications. Fluoroapatites are

*Corresponding author. Fax: +39 051 2099456.
*E-mail address:* gazzano@isof.cnr.it (M. Gazzano).

0022-4596/$ - see front matter © 2006 Elsevier Inc. All rights reserved.
doi:10.1016/j.jssc.2006.06.001

known for the bivalent metals $M = Ca$, Sr, Ba and Pb [16–18], and bicationic systems of Sr-, Cd- and Pb-substituted Ca fluoroapatites have been widely investigated [19–21]. The limit of miscibility for these systems was correlated to the relative properties of the metals, such as polarizability, electronegativity and cationic size [22,23]. The lattice parameters of the mixed apatites generally decrease with increasing content of the smaller metal cation, and in the case of the Ca–Sr and Ca–Pb systems, the results of powder pattern fitting refinement indicate a clear preference of $Ca^{2+}$ to the site $M(1)$ of the apatitic structure [19,21]. In contrast, in Ca–Cd fluoroapatites, the smaller $Cd^{2+}$ cation prefers the $M(2)$ site [24]. To the best of our knowledge, no other mixed bivalent-metal fluoroapatites have been reported. Herein we report the results of a structural and spectroscopic investigation carried out on solid solutions of mixed lead–strontium fluoroapatites (PbSrFAp) in order to study the fluoroapatite structural modifications as a function of cationic composition.

## 2. Experimental

### 2.1. Synthesis

The chemicals used for the preparation of these samples were either Riedel-de Haen AG or Fluka extra pure grade. The mixed lead and strontium fluoroapatites $Pb_{(10-x)}Sr_xFAp$, with $x$ ranging from 0 to 10, were obtained from a double decomposition method [25,26]. Two solutions were prepared to perform the synthesis: (i) solution (A), 250 ml, containing a mixture of lead and strontium nitrate, with a total concentration of metal cations of 0.2 M; (ii) solution (B), 150 ml, containing ammonium hydrogenphosphate 0.2 M and ammonium fluoride 0.13 M. The amount of the reagents correspond to the stoichiometric amount of the desired apatite apart from fluoride ion that was added in double quantity in order to prevent the insertion of $OH^-$ ions in the apatite. Solution (A) was added dropwise on solution (B), maintained at boiling temperature, under nitrogen stream. The pH value of the slurry was maintained approximately at 11 by regular additions of small amounts of ammonia ($d = 0.89$; 28% aqueous solution). The resulting solid phase was kept in contact with the mother solution for 1 h, at boiling temperature. The precipitate was then filtered, washed with hot distilled water, dried at 100 °C for 12 h and calcined at 400 °C for 4 h to improve its crystallinity.

The formation of solid solutions of strontium-substituted lead apatites can be summarized from the chemical equation given below:

$$(10-x)Pb(NO_3)_2 + xSr(NO_3)_2 + 6(NH_4)_2HPO_4 + 6(NH_4OH) + 2(NH_4F) \rightarrow Pb_{(10-x)}Sr_x(PO_4)_6F_2 + 20NH_4NO_3 + 6H_2O.$$

### 2.2. Chemical analyses and instrumental methods

#### 2.2.1. X-ray powder diffraction (XRD)

The XRD data were collected with a Philips PW1710 diffractometer, equipped with a copper anode and a graphite monochromator in the diffracted beam ($K_\alpha$ radiation, $\lambda = 1.5418$ Å); $2\theta$ range 10–100°, step width 0.03° and counting time 10 s.

#### 2.2.2. Infrared (IR) analysis

The IR absorption spectra have been recorded on a Fourier transform spectrometer BIORAD (FTC 6000), whose spectral domain spreads from 4000 to 250 $cm^{-1}$. One milligram of the samples was crushed with 300 mg of KBr, and pelletized at 12 tons [27].

#### 2.2.3. Chemical analysis

The lead and strontium concentrations of the solid products were determined with a Perkin Elmer 3110 atomic absorption spectrophotometer. The phosphate ions were quantified by visible absorption spectrophotometry of the phosphovanadomolybdic complex. The measurement of the optical densities was carried out at 400 nm [28]. Fluoride content was determined by potentiometry, using an ionometer equipped with a fluoride-specific electrode, at ambient temperature and pH ca. 6. The support electrolyte was 1 M aqueous solution of sodium citrate.

#### 2.2.4. Structural analysis

The DBWS-9411 program [29,30] was used to refine the structures of the mixed lead–strontium fluoroapatites. The space group ($P6_3/m$, n. 176), the cell parameters, the atomic positions and the Debye–Waller factors of PbFAp are introduced as the initial structural model for the fluoroapatites with the lowest strontium content [18]. A five order polynomial was used to simulate the background, while the peaks were fitted by using a "pseudo-Voigt" function. Half width of the diffraction peaks as a function of $2\theta$ was evaluated by the formulation of the Caglioti model [31]. Rietveld refinement was performed in several stages. In the first cycles, the scale factor and the background were refined. Refinement of the other parameters is in the following order: profile parameters, zero shift, asymmetry parameter and cell parameters. Refinement of the occupancy factors was done only for $Pb^{2+}$ and $Sr^{2+}$ ions, with the assumption that these two cations are, initially, statistically located in the two cationic sites, the total contents constrained to the stoichiometry obtained by chemical analysis. The coordinates were refined, starting with those of the two metal sites. In the last refinement cycles, all 30 parameters are released. Then, the refined parameters were used as the initial model for apatite with strontium content immediately greater, and so on. The geometrical calculations were carried on with the help of the DIAMOND program [32]. Further details of the crystal structure investigations can be obtained from the Fachinformationszentrum Karlsruhe, 76344

Eggenstein-Leopodshafen, Germany (e.mail: crysdata@fiz.karlsruhe), on quoting the depository numbers CSD 416381/416385. The structural data of SrFAp were reported in a previous paper [33].

## 3. Results and discussion

### 3.1. Chemical analysis

The results of the chemical analysis reported in Table 1 are consistent with the formation of solid solutions of PbSrFAp. The atomic ratios (Sr + Pb)/P are close to the stoichiometric value of 1667 for apatites. The relative content of the two metallic cations in the solid products is very close to that in the synthesis solutions. The mixed fluoroapatites are indicated as $Pb_{(10-x)}Sr_xFAp$, where $x$ corresponds to the value used in the synthesis.

### 3.2. X-ray analysis

The XRD patterns (two of which are reported as an example in Fig. 1) show that all the samples are single-phase fluoroapatites. The structural refinements allow the determination of unit cell dimensions. Their values indicate the formation of a continuous solid solution of lead–strontium fluoroapatites. The variation of the parameters is essentially linear (Fig. 2) and follows the Végard law [34] according to the following equations:

$$a = (0.97714 - 0.00052x)\ (\text{nm}), \quad \sigma(a) = 0.0004\ (\text{nm}),$$
$$c = (0.72938 - 0.00008x)\ (\text{nm}), \quad \sigma(c) = 0.0070\ (\text{nm}),$$

where $x$ is the molar content of strontium. The replacement of lead by the strontium cation induces a decrease of the lattice parameter "$a$" in the apatitic structure, but it does not affect significantly the $c$-axis. Although the difference in the cationic radii is small ($Pb^{2+}$ coord. 7, radius 0.137 nm; $Sr^{2+}$ coord. 7, radius 0.135 nm), it should be the reason of the observed slight contraction of the $a$-axis.

Table 1
Result of chemical analyses of PbSrFAp solid solutions (e.s.d. in parentheses)

| $x$ (synthesis) | $x$ (chemical analysis) | $P$ content/cell | Atom ratio (Pb + Sr)/P | $F^-$ content/cell |
|---|---|---|---|---|
| 0.0 | 0.0 | 5.96(4) | 1.67(5) | 1.89(2) |
| 1.0 | 1.09(2) | 5.95(3) | 1.68(2) | 1.90(2) |
| 2.0 | 1.95(2) | 5.96(3) | 1.67(4) | 1.95(4) |
| 3.0 | 2.92(3) | 5.95(4) | 1.68(3) | 1.96(1) |
| 4.0 | 3.96(1) | 5.93(2) | 1.68(2) | 1.93(2) |
| 5.0 | 4.94(2) | 5.96(2) | 1.67(4) | 1.98(3) |
| 6.0 | 6.04(4) | 5.97(5) | 1.67(5) | 2.03(1) |
| 7.0 | 6.98(2) | 5.97(4) | 1.67(3) | 1.93(4) |
| 8.0 | 8.08(3) | 5.93(2) | 1.68(5) | 1.91(3) |
| 9.0 | 9.11(3) | 5.96(4) | 1.67(4) | 1.89(2) |
| 10.0 | 10.01(2) | 5.98(3) | 1.67(2) | 1.97(4) |

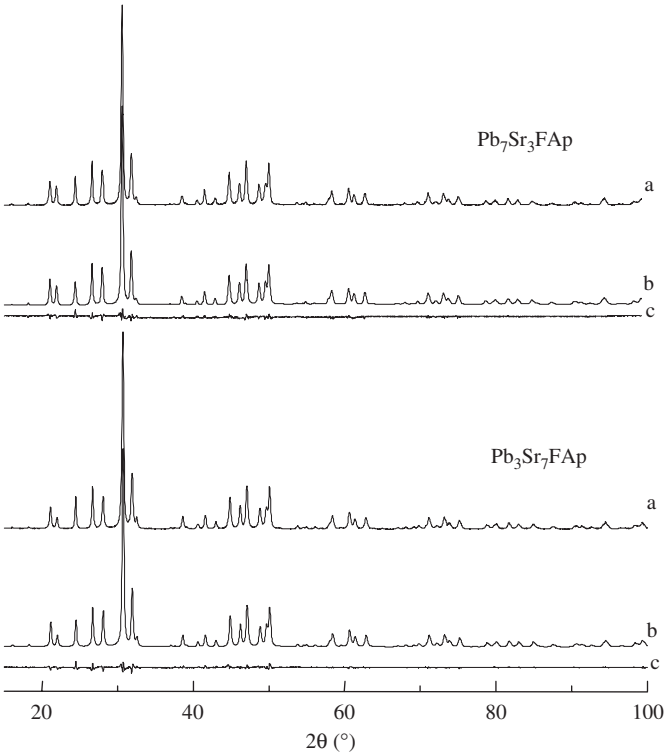


Fig. 1. Comparison of the observed [curve (a)] and calculated [curve (b)] powder diffraction patterns of $Pb_7Sr_3FAp$ and $Pb_3Sr_7FAp$. Curve (c) is the difference profile.

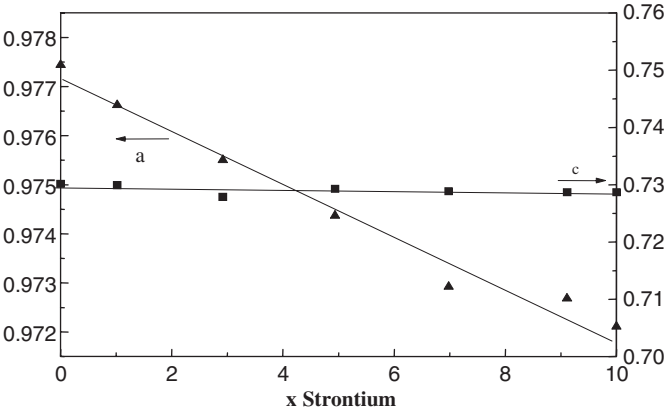


Fig. 2. Lattice constants of the solid solution in the Pb–Sr system against the strontium molar content.

Fig. 1 displays the final plot for $Pb_7Sr_3FAp$ and $Pb_3Sr_7FAp$ samples, as typical comparisons between the observed and calculated patterns. The unit cell dimensions and the atomic positions of five apatites with different atomic Pb/Sr ratio are reported in Table 2.

Although the scattering contribution of fluoride to the total diffraction is small, the data reported for several samples indicate a trend which substantiates a fluoride

Table 2
Lattice parameters (nm), agreement indexes and fractional atomic coordinates after Rietveld refinement, for the mixed PbSrFAp (e.s.d. in parentheses)

| | *x* | *y* | *z* |
|---|---|---|---|
| $Pb_9Sr_1FAp$ | $a = 0.97662(4)$, $c = 0.72929(2)$, $V = 0.60303(3)$, $R_p = 8.2$, $R_{wp} = 10.9$ | | |
| *M*(1) | 0.3333 | 0.6667 | −0.0091(1) |
| *M*(2) | 0.2375(1) | 0.0036(6) | 0.2500 |
| P | 0.4122(2) | 0.3834(5) | 0.2500 |
| O(1) | 0.322(2) | 0.459(5) | 0.2500 |
| O(2) | 0.552(4) | 0.464(3) | 0.2500 |
| O(3) | 0.357(5) | 0.288(2) | 0.067(2) |
| F | 0.0000 | 0.0000 | 0.449(3) |
| $Pb_7Sr_3Fap$ | $a = 0.97550(4)$, $c = 0.72787(2)$, $V = 0.60002(5)$, $R_p = 7.8$, $R_{wp} = 10.0$ | | |
| *M*(1) | 0.3333 | 0.6667 | 0.0074(4) |
| *M*(2) | 0.2421(1) | 1.0032(3) | 0.2500 |
| P | 0.4052(2) | 0.3797(4) | 0.2500 |
| O(1) | 0.345(1) | 0.499(4) | 0.2500 |
| O(2) | 0.592(4) | 0.505(7) | 0.2500 |
| O(3) | 0.357(3) | 0.273(4) | 0.093(3) |
| F | 0.0000 | 0.0000 | 0.326(5) |
| $Pb_5Sr_5FAp$ | $a = 0.97437(5)$, $c = 0.72928(3)$, $V = 0.59956(4)$, $R_p = 6.4$, $R_{wp} = 8.3$ | | |
| *M*(1) | 0.3333 | 0.6667 | −0.0001(3) |
| *M*(2) | 0.2406(2) | 0.9888(1) | 0.2500 |
| P | 0.3988(4) | 0.3782(3) | 0.2500 |
| O(1) | 0.3408(5) | 0.4664(2) | 0.2500 |
| O(2) | 0.5804(8) | 0.4549(3) | 0.2500 |
| O(3) | 0.3462(5) | 0.2695(2) | 0.093(5) |
| F | 0.0000 | 0.0000 | 0.299(2) |
| $Pb_3Sr_7FAp$ | $a = 0.97292(3)$, $c = 0.72888(1)$, $V = 0.59757(2)$, $R_p = 6.0$, $R_{wp} = 7.8$ | | |
| *M*(1) | 0.3333 | 0.6667 | −0.0018(4) |
| *M*(2) | 0.2398(2) | 0.9869(5) | 0.2500 |
| P | 0.3986(4) | 0.3754(3) | 0.2500 |
| O(1) | 0.337(2) | 0.473(3) | 0.2500 |
| O(2) | 0.588(2) | 0.464(1) | 0.2500 |
| O(3) | 0.347(4) | 0.267(2) | 0.088(3) |
| F | 0.0000 | 0.0000 | 0.286(6) |
| $Pb_1Sr_9FAp$ | $a = 0.97268(3)$, $c = 0.72871(1)$, $V = 0.59673(2)$, $R_p = 5.6$, $R_{wp} = 7.4$ | | |
| *M*(1) | 0.3333 | 0.6667 | −0.0020(4) |
| *M*(2) | 0.2397(1) | 0.9854(2) | 0.2500 |
| P | 0.3991(3) | 0.3713(3) | 0.2500 |
| O(1) | 0.336(4) | 0.479(5) | 0.2500 |
| O(2) | 0.582(4) | 0.462(4) | 0.2500 |
| O(3) | 0.342(7) | 0.261(2) | 0.079(4) |
| F | 0.0000 | 0.0000 | 0.274(3) |

$R_p = 100[\Sigma|Y_{oi}-Y_{ci}|/\Sigma Y_{oi}]$, $R_{wp} = 100[W_i(Y_{oi}-Y_{ci})^2/\Sigma W_i(Y_{oi})^2]^{1/2}$.

displacement as strontium content increases. Examination of Table 2 shows that the position of the fluoride ion shifts progressively along the *c*-axis direction. In the apatitic channel of lead apatite, the $F^-$ ions are positioned very close to the mid point between the planes of the *M*(2) triangles ($z = \frac{1}{2}$). As the Sr/Pb ratio increases, the fluoride ions move regularly towards the centre of *M*(2) triangles ($z = \frac{1}{4}$), that is reached in the $Sr_{10}FAp$ as sketched in Fig. 3.

A similar phenomenon was observed for the displacement of the $OH^-$ ion in the calcium–lead and cadmium–lead hydroxyapatite series [35–36]. The substitution of calcium or cadmium for lead causes a shift of the $OH^-$ group position towards the centre of *M*(2) triangles. In those cases, the driving force was ascribed to the ionic radii difference. Indeed, when the site *M*(2) is mainly occupied by Pb atoms, the space at the centre of *M*(2) triangles is reduced significantly and the hydroxyl ion must be accommodated outside. In the present case, the effect is even more evident, but difference in ionic size cannot be invoked, because of the similarity of $Pb^{2+}$ and $Sr^{2+}$ radii. As a matter of fact, lead is a soft acid and displays a greater tendency towards covalent interactions and directional bonding, whereas strontium can be considered a hard acid, and it could display a greater affinity for $OH^-$, a hard base

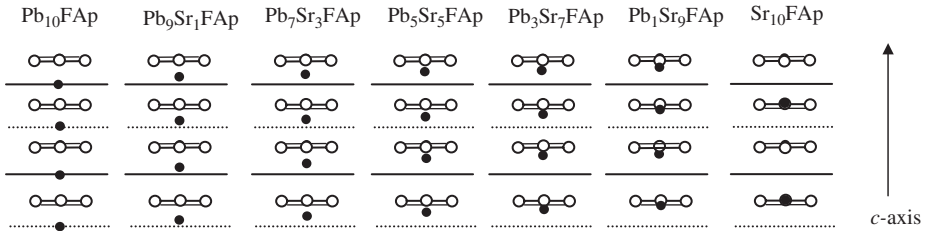


Fig. 3. A view of the fluoride position perpendicular to the *c*-axis in PbSrFAp. White circles represents *M*(2) sites, black circles fluoride atoms.

Table 3
Statistic distribution and refined occupancy of strontium atoms in the two metal sites *M*(1) and *M*(2) of PbSrFAp

| | Distribution from refinement (*A*) | | Statistic distribution (*B*) | | (*A*−*B*/*B*) | |
|---|---|---|---|---|---|---|
| | *M*(1) | *M*(2) | *M*(1) | *M*(2) | *M*(1) | *M*(2) |
| $Pb_9Sr_1FAp$ | 0.70 | 0.32 | 0.41 | 0.61 | +0.71 | −0.47 |
| $Pb_7Sr_3FAp$ | 1.92 | 1.11 | 1.22 | 1.82 | +0.58 | −0.39 |
| $Pb_5Sr_5FAp$ | 2.41 | 2.58 | 1.99 | 2.99 | +0.21 | −0.14 |
| $Pb_3Sr_7FAp$ | 3.01 | 3.98 | 2.79 | 4.20 | +0.08 | −0.05 |
| $Pb_1Sr_9FAp$ | 3.76 | 5.32 | 3.64 | 5.46 | +0.03 | −0.02 |

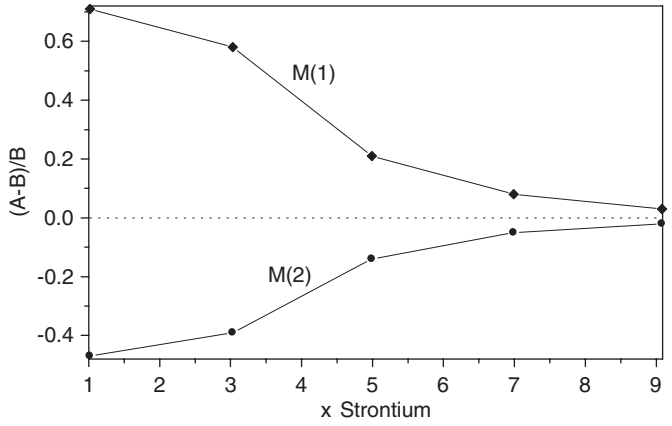


Fig. 4. Relative difference distribution of strontium atoms between *M*(1) and *M*(2) crystallographic sites.

[37]. $F^-$ ion, which is smaller than $OH^-$, is a hard base as well, which can account for the shift caused by strontium substitution to lead in fluoroapatite.

The refinement of the occupation factors indicate that the $Sr^{2+}$ ions are distributed between the two crystallographic sites *M*(1) and *M*(2), with a preference for the smaller site M(1) (Table 3). This is appreciable for low strontium concentrations (see Fig. 4). The corresponding occupation of the *M*(1) is always greater than the statistical distribution and the difference with the statistical distribution decreases when the overall strontium content increases, similarly to what previously found for SrPbHOAp [38].

Table 4 reports the interatomic distances. The values of the mean *M*(1)–O and *M*(2)–O distances slightly decrease as the amount of strontium in the fluoroapatite increases, in agreement with the reduction of the *a*-axis. The *M*(2)–F distance is the most affected from the variation in the composition due to the shift of $F^-$ ions towards the centre of the triangle formed by *M*(2) atoms as the strontium content increases. All samples display P–O distances within the typical values for orthophosphates [39]. The variation of the *M*(1)–*M*(2) distances is significantly greater than those of *M*(1)–*M*(1) or *M*(2)–*M*(2) because the contraction of the unit cell, as the strontium content increases, determines the approach of metal columns, metal triangles and phosphate ions without significant structural distortion.

### 3.3. IR investigation

All the samples show IR absorption spectra typical of fluoroapatites; some of them are reported in Fig. 5. The absence of the bands due to $OH^-$, $CO_3^{2-}$ and $HPO_4^{2-}$ions indicates the absence of appreciable amount of impurities.

The IR spectra of the mixed fluoroapatites show the characteristic absorption bands (stretching and bending) of the $(PO_4)^{3-}$ group and the band at ca. 300 $cm^{-1}$ assigned to the "$\nu_3$" type stretching of the [*M*(2)$_3$–F] group [40,41]. The variation of this last band is coherent with the increase of the distance between $F^-$ ion and *M*(2) triangles on increasing lead content (Table 4). As a matter of fact, as lead substitution for strontium increases, the $\nu_3$ band shifts into two or three components, in agreement with an increase of disorder and it is no longer appreciable for samples containing more than 50% lead atoms.

Table 4
*M*–O, *M*–F and *M*–*M* distances in mixed PbSrFAp (nm × 10, e.s.d. in parentheses)

| | $Pb_{10}$FAp | $Pb_9Sr_1$FAp | $Pb_7Sr_3$FAp | $Pb_5Sr_5$FAp | $Pb_3Sr_7$FAp | $Pb_1Sr_9$FAp | $Sr_{10}$FAp |
|---|---|---|---|---|---|---|---|
| *M*(1)–O(1) × (3) | 2.55(3) | 2.52(2) | 2.50(2) | 2.65(3) | 2.64(5) | 2.60(7) | 2.56(2) |
| *M*(1)–O(2) × (3) | 2.76(3) | 2.68(2) | 2.75(3) | 2.54(3) | 2.53(3) | 2.55(2) | 2.57(6) |
| *M*(1)–O(3) × (3) | 2.86(4) | 2.92(2) | 2.92(2) | 2.93(4) | 2.92(3) | 2.93(4) | 2.91(33 |
| ⟨ *M*(1)–O ⟩ | 2.72 | 2.71 | 2.72 | 2.70 | 2.70 | 2.69 | 2.68 |
| *M*(2)–O(1) | 2.98(5) | 3.04(2) | 3.00(2) | 2.86(1) | 2.79(3) | 2.77(2) | 2.75(2) |
| *M*(2)–O(2) | 2.37(3) | 2.36(1) | 2.37(7) | 2.57(3) | 2.51(3) | 2.52(4) | 2.52(4) |
| *M*(2)–O(3) × (2) | 2.62(1) | 2.61(1) | 2.57(5) | 2.63(7) | 2.58(3) | 2.53(2) | 2.50 (3) |
| *M*(2)–O(3) × (2) | 2.64(3) | 2.65(1) | 2.66(4) | 2.65(4) | 2.64(4) | 2.66(1) | 2.68 (2) |
| ⟨ *M*(2)–O ⟩ | 2.64 | 2.65 | 2.64 | 2.66 | 2.62 | 2.61 | 2.61 |
| *M*(2)–F | 2.94(4) | 2.64(4) | 2.59(3) | 2.44(4) | 2.43(2) | 2.42(3) | 2.40 |
| *M*(2)–*M*(2) | 4.17(7) | 4.17((2) | 4.16(4) | 4.16(7) | 4.16(5) | 4.17(1) | 4.16(2) |
| *M*(1)–*M*(2) | 4.23(5) | 4.15(2) | 4.13(4) | 4.11(6) | 4.09(5) | 4.08(3) | 4.07(8) |
| *M*(1)–*M*(1) | 3.67(2) | 3.54(1) | 3.58(4) | 3.61(7) | 3.61(3) | 3.61(6) | 3.63(5) |

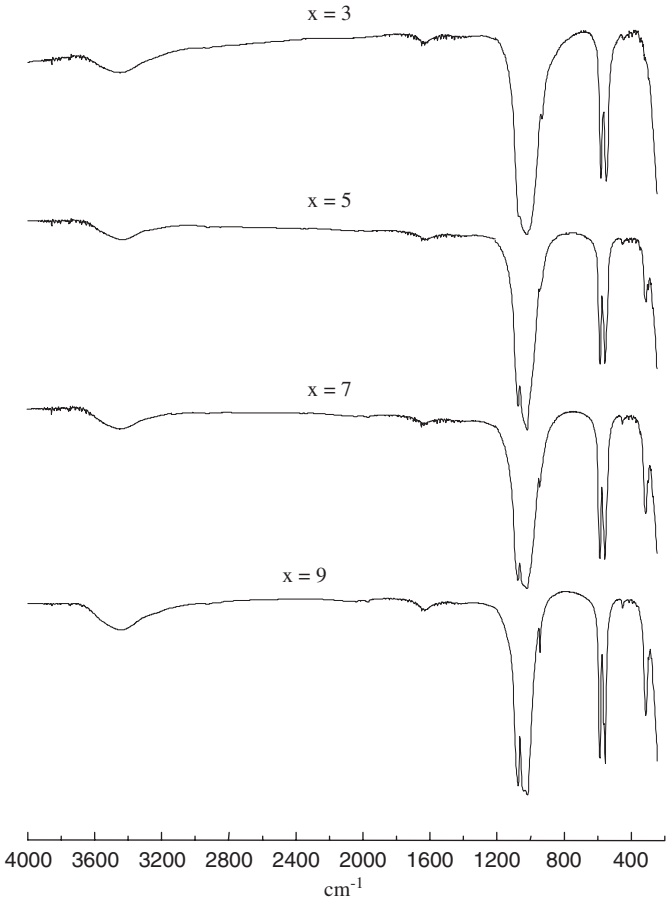


Fig. 5. Infrared spectra of mixed $Pb_{(10-x)}Sr_x(PO_4)_6F_2$.

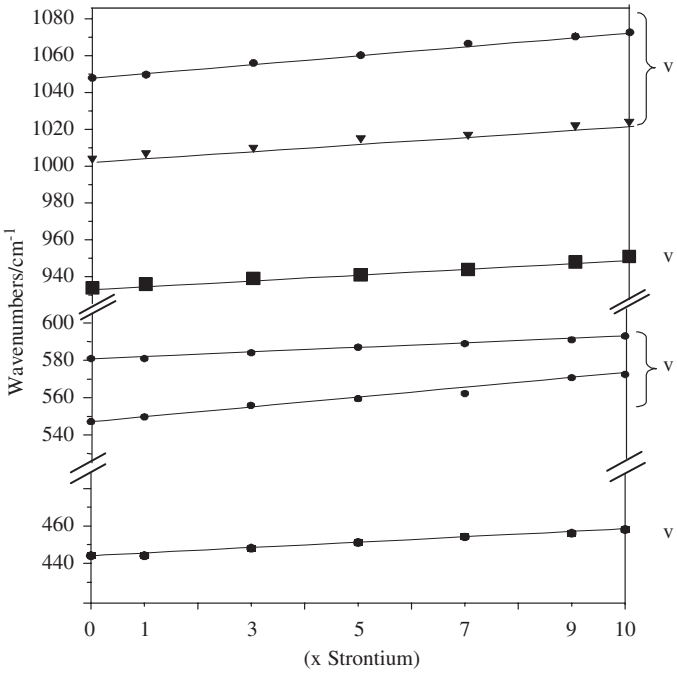


Fig. 6. Infrared frequencies of the vibrational modes of PbSrFAp solid solutions as a function of strontium content.

Moreover, the progressive replacement of the lead ions by strontium induces a regular shift of all the absorption bands towards greater wavenumbers (Fig. 6 and Table 5).

As noted by Fowler [40,41], who studied pure Ca and Sr hydroxyapatites, the increase of the frequencies of the $PO_4$ internal vibration modes might be due to increased anion–anion repulsions concomitant with decreased lattice dimensions, as also to higher covalence of the P–O bonds resulting from increased ionicity of the *M*–O bonds [23]. The splitting of the triply degenerate $\nu_3$, $\nu_4$ bands and the intensity of the $\nu_1$ and $\nu_2$ remain nearly constant over the whole series, in agreement with the minor geometrical perturbations of the $PO_4$ group, but a continuous slight

Table 5
Positions of the main infrared bands ($cm^{-1}$) for $Pb_{(10-x)}Sr_x(PO_4)_6F_2$

| $Pb_{(10-x)}Sr_xFAp$ | $\nu_1$ [$PO_4$] | $\nu_2$ [$PO_4$] | $\nu_3$ [$PO_4$] | $\nu_4$ [$PO_4$] | $\nu_3$[M(2)$_3$–F] |
|---|---|---|---|---|---|
| $Pb_9Sr_1FAp$ | 930 | 444 | 1047–997 | 577–546 | * |
| $Pb_7Sr_3FAp$ | 934 | 448 | 1073–1023 | 584–551 | * |
| $Pb_5Sr_5FAp$ | 947 | 451 | 1076–1023 | 590–559 | 322–316–302 |
| $Pb_3Sr_7FAp$ | 948 | 455 | 1077–1022 | 591–558 | 317–302 |
| $Pb_1Sr_9FAp$ | 949 | 456 | 1079–1022 | 592–561 | 321 |

broadening of the absorption bands is evident as the lead content increases.

## 4. Conclusion

The results of this study indicate that the weak difference between cationic radius of $Pb^{2+}$ and $Sr^{2+}$ ions allows the formation of a continuous solid solution of lead and strontium fluoroapatites in the whole compositional range. The progressive incorporation of the $Sr^{2+}$ cation in the lead fluoroapatite induces a contraction of the "*a*" lattice constant. Lead is a soft acid and displays a greater tendency towards covalent interactions and directional bonding, whereas strontium can be considered a hard acid. The less covalent character of Sr–O bonds, added to the decrease of lattice parameters, can be invoked to justify the net shift of the infrared $PO_4$ absorption modes towards higher frequencies. Structural refinements by Rietveld method show that the $Sr^{2+}$ ions are distributed between the two crystallographic sites *M*(1) and *M*(2), with a low preference to the smaller site *M*(1). This is particularly marked for low $Sr^{2+}$ concentrations. Furthermore, the substitution provokes the displacement of $F^-$ ions from $z \cong \frac{1}{2}$ (PbFAp) to $z \cong \frac{1}{4}$ (SrFAp) in agreement with the absence of the $\nu_3$ stretching IR band due to [$M(2)_3$–F] for apatites containing more than 50% lead atoms.

## Acknowledgment

This research was carried out with the financial support of MIUR and the University of Bologna (Funds for Selected Research Topics).

## References

[1] J.C. Elliott, Structure and Chemistry of the Apatites and Other Calcium Orthophosphates, Elsevier, Amsterdam, 1994.
[2] D. McConnel, Apatites, Applied Mineralogy, vol. 5, Springer, New York, Vienna, 1963.
[3] G. Wright, G. Montel, C.R. Acad. Sci. 268C (1969) 2077–2080.
[4] M.I. Kay, R.A. Young, A.S. Posner, Nature 204 (1964) 1050–1052.
[5] Z. Opre, J.D. Grunwaldt, T. Mallat, A. Baiker, J. Mol. Catal. A Chem. 242 (2005) 224–232.
[6] S.G. Dahl, P. Allain, P.J. Marie, Y. Mauras, G. Boivin, P. Ammann, Y. Tsouderos, P.D. Delmas, C. Christiansen, Bone 28 (2001) 446–453.
[7] J.C. Elliott, Calcium phosphate biominerals, in: M.J. Kohn, J. Rakovan, J.M. Hughes (Eds.), Phosphates: Geochemical, Geobiological and Material Importance, Reviews in Mineralogy and Geochemistry, vol. 48, Mineralogical Society of America, Washington, 2002, pp. 427–454.
[8] R.Z. LeGeros, Calcium phosphates in oral biology and medicine, in: H.M. Myers (Ed.), Monographs in Oral Science, Karger Publishing, New York, 1991.
[9] T. Yamamuro, L.L. Hench, J. Wilson (Eds.), CRC Handbook of Bioactive Ceramics, vol. II—Calcium Phosphates and Hydroxyapatites Ceramics, CRC Press, Boca Raton, FL, 1990.
[10] P. Becker, in: Fertilizer Science and Technology Series, Marcel Dekker, New York, 1989, pp. 6–20.
[11] J. Boisson, A. Rotten, M. Mench, J. Vangronsveld, Environ. Pollut. 104 (1999) 225–233.
[12] Y. Matsumura, S. Sugiyama, H.J.B. Hayashi, J.B. Moffat, J. Solid State Chem. 114 (1995) 138–145.
[13] D.K. Sardar, F. Castano, J. Appl. Phys. 91 (2002) 911–915.
[14] A. Laghzizil, N.E. Herch, A. Bouhaouss, G. Lorente, J. Macquete, J. Solid State Chem. 156 (2001) 57–60.
[15] J.M. Hughes, J. Rakovan, The crystal structure of apatite, $Ca_5(PO_4)_3(F,OH,Cl)$, in: M.J. Kohn, J. Rakovan, J.M. Hughes (Eds.), Phosphates: Geochemical, Geobiological and Material Importance, Reviews in Mineralogy and Geochemistry, vol. 48, Mineralogical Society of America, Washington, DC, 2002, pp. 1–12.
[16] E.L. Belokoneva, E.A. Troneva, L.N. Demyanets, N.G. Duderov, N.V. Belov, Kristallografiya 27 (1982) 793–794.
[17] E.R. Kreidler, F.A. Hummel, Am. Mineral. 55 (1970) 170–187.
[18] M. Mathew, I. Mayer, B. Dickens, L.W. Schroeder, J. Solid State Chem. 28 (1979) 79–95.
[19] I. Khattech, M. Jemal, Thermochim. Acta 298 (1997) 23–30.
[20] A. Nounah, J.L. Lacout, J. Solid State Chem. 107 (1993) 444–451.
[21] I. Ntahomvukiye, I. Khattech, M. Jemal, Ann. Chim.-Paris 22 (1997) 435–446.
[22] A. Hamad, B. Badraoui, M. Debbabi, J. Soc. Chim. Tunisie 5 (2003) 115–124.
[23] A.A. Hamad, B. Badraoui, M. Debbabi, J. Soc. Alger. Chim. 13 (2003) 131–140.
[24] O.E. Piro, M.C. Apella, E.J. Baran, B.E. Rivero, Rev. Chim. Minér. 19 (1982) 11–18.
[25] A. Nounah, J. Szeilagyi, J.L. Lacout, Ann. Chim. Fr. 15 (1990) 409–419.
[26] A. Bigi, M. Gazzano, A. Ripamonti, E. Foresti, N. Roveri, J. Chem. Soc. Dalton Trans. (1986) 241–244.
[27] R.N. Hannah, J.S. Swinehart, Experiments in Technique of Infrared Spectroscopy, Perkin-Elmer, Norwalk, Connecticut, 1974.
[28] K.P. Quinlan, M.A. De Sesa, Anal. Chem. 27 (1955) 1626–1629.
[29] M. Rietveld, J. Appl. Crystallogr. 2 (1969) 65–71.
[30] R.A. Young, A. Sakthivel, T.S. Moss, C.O. Paiva Santos, J. Appl. Crystallogr. 28 (1995) 366–367.

[31] G. Caglioti, A. Paoletti, F.P. Ricci, Nucl. Instrum. 3 (1958) 223–228.
[32] K. Brandenburg, DIAMOND, Crystal Structure Information System, Version 1.2., 1997.
[33] A. Aissa, B. Badraoui, R. Thouvenot, M. Debbabi, Eur. J. Inorg. Chem. (2004) 3828–3836.
[34] L. Végard, Z. Phyzik 9 (1922) 395–410.
[35] B. Badraoui, A. Bigi, M. Debbabi, M. Gazzano, N. Roveri, R. Thouvenot, Eur. J. Inorg. Chem. (2001) 1261–1267.
[36] A. Bigi, M. Gandolfi, M. Gazzano, A. Ripamonti, N. Roveri, S.A. Thomas, J. Chem. Soc. Dalton Trans. (1991) 2883–2886.
[37] R.G. Pearson, Inorg. Chem. 27 (1988) 734–740.
[38] B. Badraoui, A. Bigi, M. Debbabi, M. Gazzano, N. Roveri, R. Thouvenot, Eur. J. Inorg. Chem. (2002) 1864–1870.
[39] W.H. Baur, Acta Crystallogr. B 30 (1974) 1195–1215.
[40] B.O. Fowler, Inorg. Chem. 13 (1974) 207–214.
[41] B.O. Fowler, Inorg. Chem. 13 (1974) 194–207.